**Cell Reports, Volume *30***

## Supplemental Information

# FMRP Control of Ribosome Translocation Promotes Chromatin Modifications and Alternative Splicing of Neuronal Genes Linked to Autism

**Sneha Shah, Gemma Molinaro, Botao Liu, Ruijia Wang, Kimberly M. Huber, and Joel D. Richter**

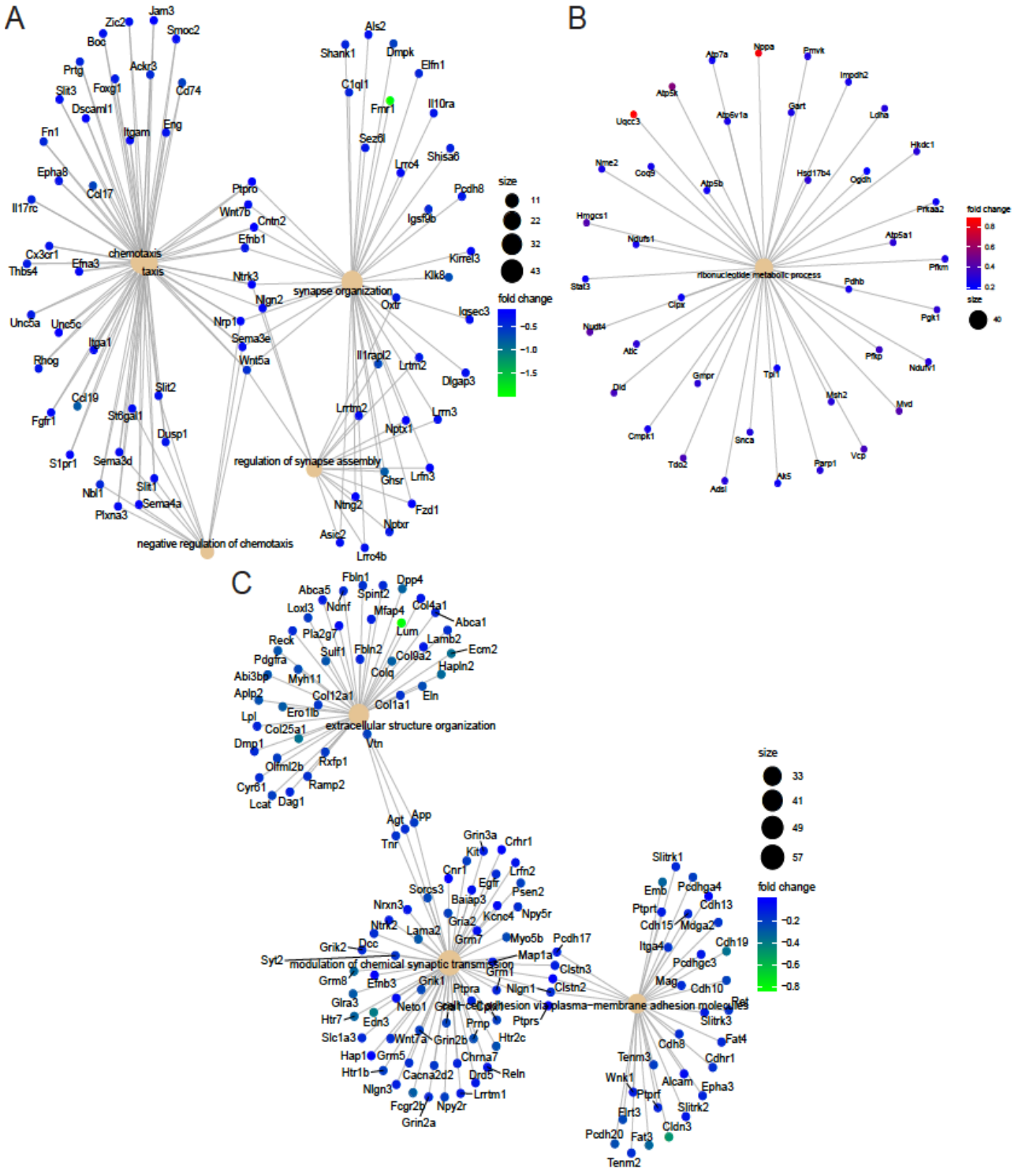
A
chemotaxis
taxis
synapse organization
regulation of synapse assembly
negative regulation of chemotaxis
size
fold change
B
ribonucleotide metabolic process
fold change
size
C
extracellular structure organization
modulation of chemical synaptic transmission
cell-cell adhesion via plasma-membrane adhesion molecules
size
fold change

**Figure S1. Clustering of RNAs with changes in TE and mRNA abundance to identify functional hubs (Related to Figure 1, also see TableS1)**

(A) Network clustering of "mRNA up" RNAs from the ribosome profiling and RNA-seq in WT and *Fmr1* KO hippocampus. Nodes indicate the functional processes linked to the RNAs identified. Fold changes are indicated.

(B) Network clustering of the functional processes in the "mRNA down" RNAs

(C) Network analysis of the of the functional processes in the "TE down" mRNAs

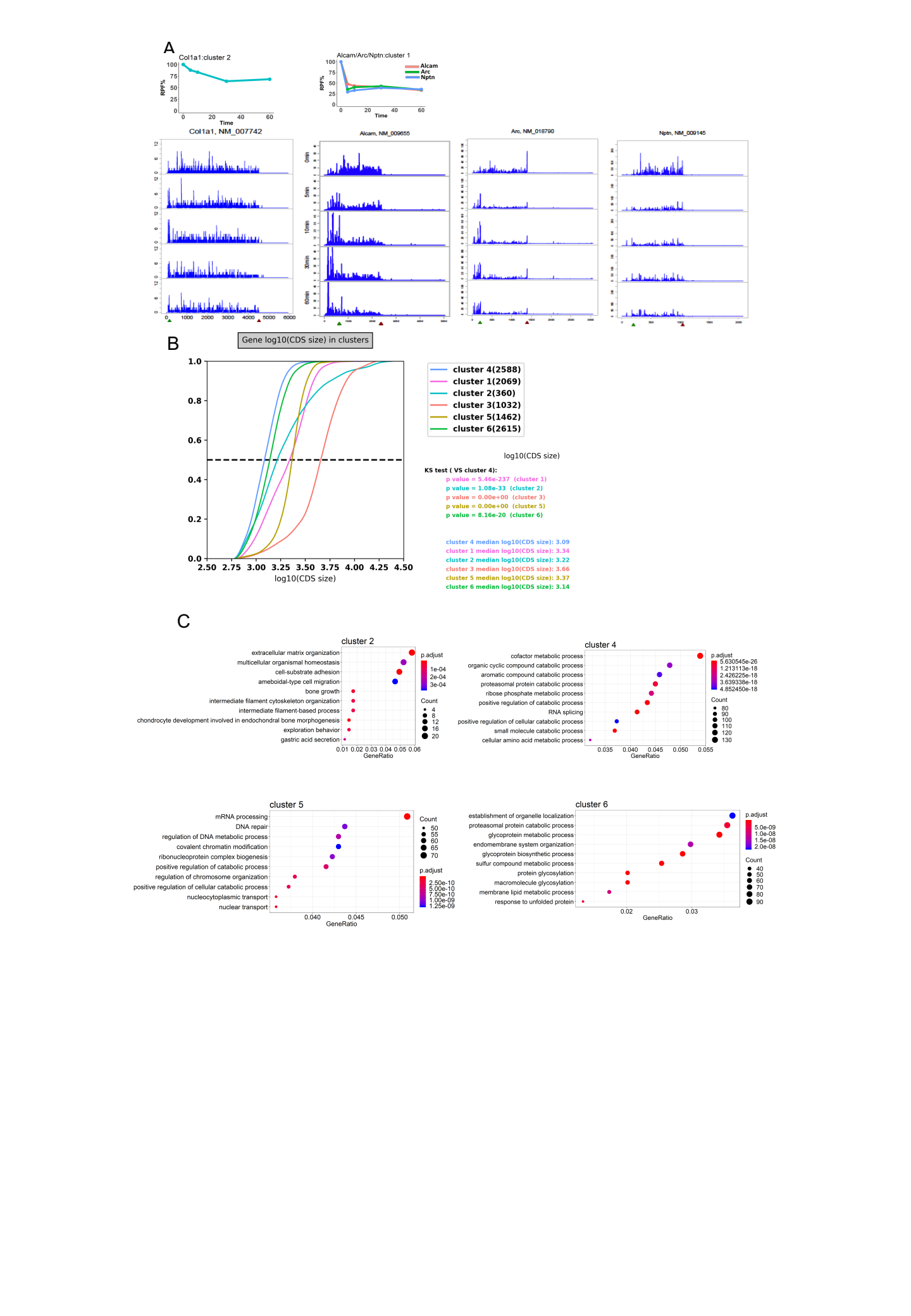
A
Col1a1:cluster 2
Alcam/Arc/Nptn:cluster 1
Alcam
Arc
Nptn
RPF%
Time
Col1a1, NM_007742
Alcam, NM_009655
Arc, NM_018790
Nptn, NM_009145
0min
5min
10min
30min
60min
B
Gene log10(CDS size) in clusters
cluster 4(2588)
cluster 1(2069)
cluster 2(360)
cluster 3(1032)
cluster 5(1462)
cluster 6(2615)
log10(CDS size)
KS test ( VS cluster 4):
p value = 5.46e-237 (cluster 1)
p value = 1.08e-33 (cluster 2)
p value = 0.00e+00 (cluster 3)
p value = 0.00e+00 (cluster 5)
p value = 8.16e-20 (cluster 6)
cluster 4 median log10(CDS size): 3.09
cluster 1 median log10(CDS size): 3.34
cluster 2 median log10(CDS size): 3.22
cluster 3 median log10(CDS size): 3.66
cluster 5 median log10(CDS size): 3.37
cluster 6 median log10(CDS size): 3.14
C
cluster 2
extracellular matrix organization
multicellular organismal homeostasis
cell-substrate adhesion
ameboidal-type cell migration
bone growth
intermediate filament cytoskeleton organization
intermediate filament-based process
chondrocyte development involved in endochondral bone morphogenesis
exploration behavior
gastric acid secretion
p.adjust
Count
GeneRatio
cluster 4
cofactor metabolic process
organic cyclic compound catabolic process
aromatic compound catabolic process
proteasomal protein catabolic process
ribose phosphate metabolic process
positive regulation of catabolic process
RNA splicing
positive regulation of cellular catabolic process
small molecule catabolic process
cellular amino acid metabolic process
cluster 5
mRNA processing
DNA repair
regulation of DNA metabolic process
covalent chromatin modification
ribonucleoprotein complex biogenesis
positive regulation of catabolic process
regulation of chromosome organization
positive regulation of cellular catabolic process
nucleocytoplasmic transport
nuclear transport
cluster 6
establishment of organelle localization
proteasomal protein catabolic process
glycoprotein metabolic process
endomembrane system organization
glycoprotein biosynthetic process
sulfur compound metabolic process
protein glycosylation
macromolecule glycosylation
membrane lipid metabolic process
response to unfolded protein

**Figure S2. Run-off ribosome profiling of WT mouse hippocampal slices. (Related to Figure 3, also see Table S1)**

(A) Ribosome runoff patterns for clusters 1 and 2. The RPFs of each gene at each time point was normalized to time 0. The euclidean distance matrix was then calculated, followed by hierarchical clustering using Ward's agglomeration method (Ward, 1963). The global pattern of each sub-cluster was summarized using the corresponding median and standard deviation in each timepoint. Representative ribosome runoff profiles are shown.

(B) CDS length dependency of the ribosome runoff rates. Results of the K-S test for significance are shown

(C) GO terms for sub-clusters 2,4, 5 and 6.

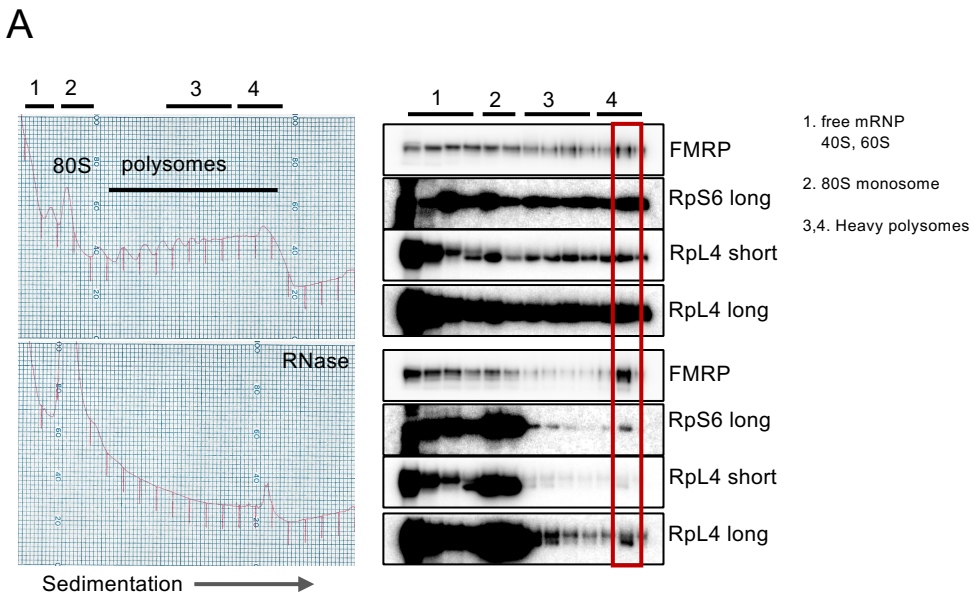
A
1
2
3
4
80S
polysomes
RNase
Sedimentation
FMRP
RpS6 long
RpL4 short
RpL4 long
1. free mRNP
40S, 60S
2. 80S monosome
3,4. Heavy polysomes

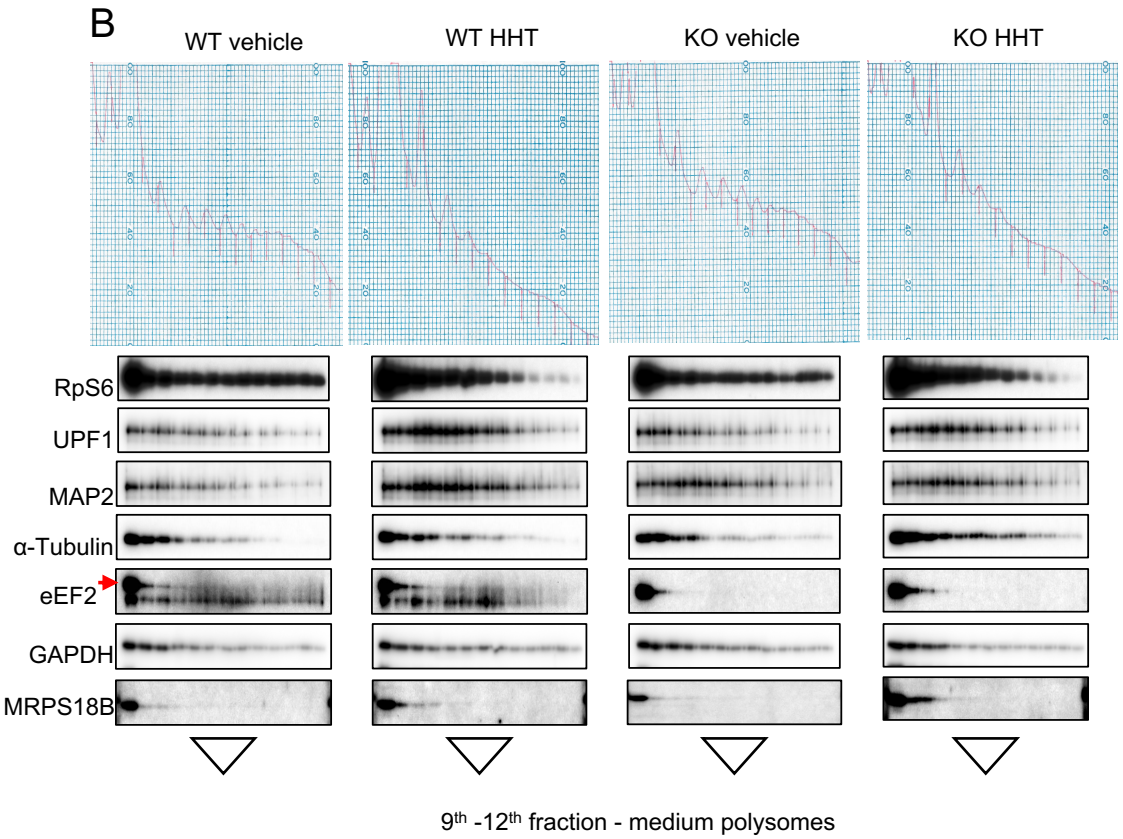
B
WT vehicle
WT HHT
KO vehicle
KO HHT
RpS6
UPF1
MAP2
α-Tubulin
eEF2
GAPDH
MRPS18B
9th -12th fraction - medium polysomes

**Figure S3. Sedimentation of proteins in polysome sucrose gradients. (Related to Figure 4, also see Table S1)**

(A) Hippocampal extracts, some of which were treated with RNAse A, were centrifuged through sucrose gradients, fractionated, and immunoblotted for FMRP, RPS6 and RPL4. Long and short refer to relative exposure times.

(B) Hippocampal slices from WT or FMRP KO mice were treated with vehicle only or HHT for 30 min. The gradients were fractionated and immunoblotted for the indicated proteins. The red arrow denotes the eEF2 band. The medium polysome fractions are indicated.

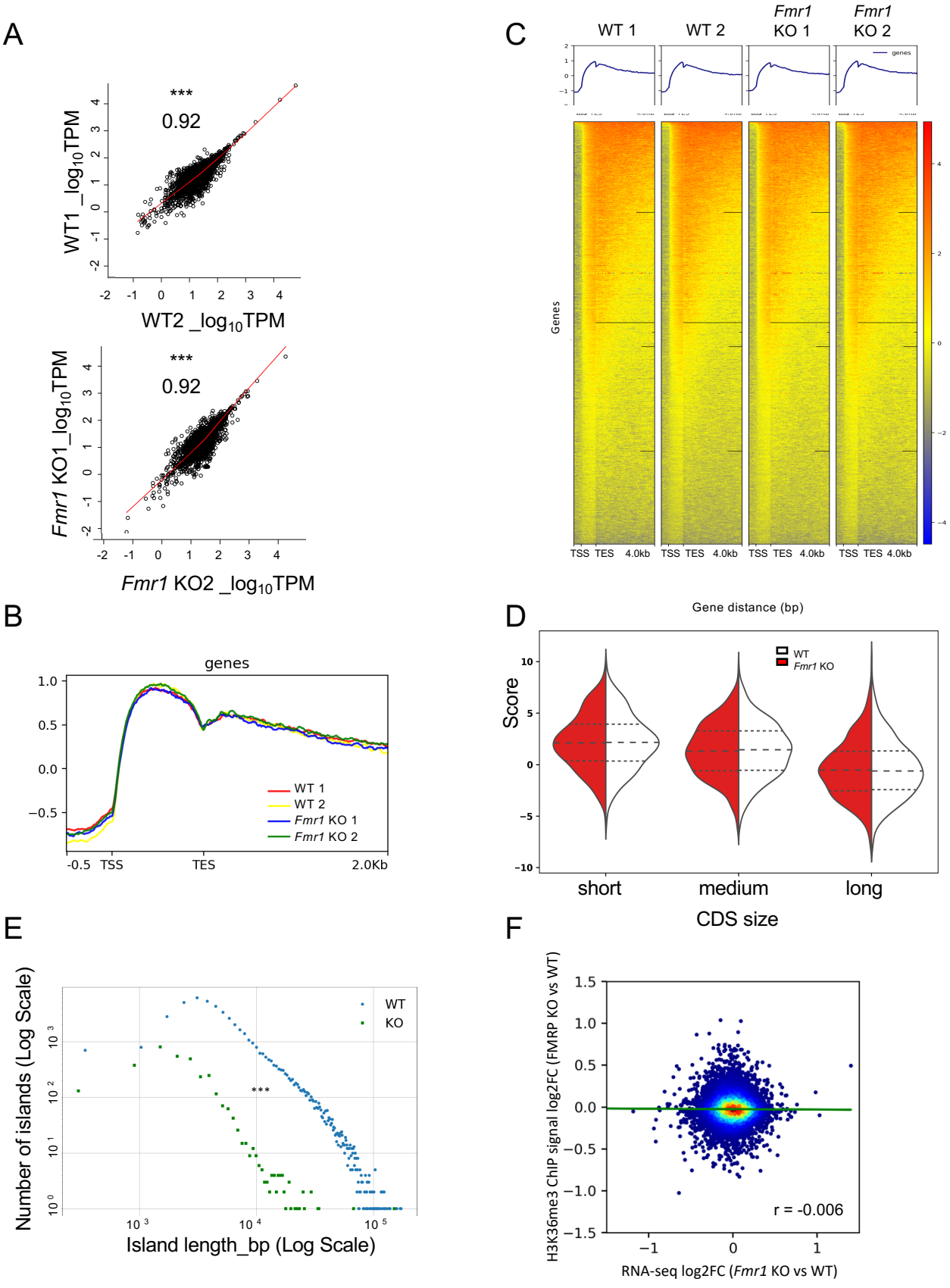
A
***
0.92
WT1 _log10TPM
WT2 _log10TPM
***
0.92
Fmr1 KO1 _log10TPM
Fmr1 KO2 _log10TPM
B
genes
WT 1
WT 2
Fmr1 KO 1
Fmr1 KO 2
-0.5 TSS
TES
2.0Kb
C
WT 1
WT 2
Fmr1 KO 1
Fmr1 KO 2
genes
Genes
TSS TES 4.0kb
D
Gene distance (bp)
WT
Fmr1 KO
Score
short
medium
long
CDS size
E
WT
KO
***
Number of islands (Log Scale)
Island length_bp (Log Scale)
F
H3K36me3 ChIP signal log2FC (FMRP KO vs WT)
r = -0.006
RNA-seq log2FC (Fmr1 KO vs WT)

**Figure S4. H3K36me3 ChIP metagene analysis (Related to Figure 6, also see Table S2)**

(A) Scatter plot for ChIP-seq normalized reads density (Transcripts per million mapped reads, TPM) mapped to the genic regions between biological replicate samples, WT1 and WT2 and *Fmr1* KO1 and *Fmr1* KO2. Pearson r values for correlation efficiency are shown. Asterisks indicate statistical significance.

(B) Metagene plots using deepTools (Ramírez et al., 2016) for distribution of H3K36me3 marks along the gene lengths. A similar increase in ChIP signal in all samples is seen in the gene body. The transcription start site (TSS), Transcription end site (TES) and 2.0kb downstream is shown.

(C) Heatmap for distribution of H3K36me3 signal along the gene length in each sample, compiled plot in Figure S4B. The transcription start site (TSS), Transcription end site (TES) and 4.0kb downstream is shown. No overall differences in ChIP signal was observed between samples.

(D) Violin plot to assess the effect of gene length on H3K36me3 ChIP signal between WT (white) and *Fmr1* KO (red) samples.

(E) Histogram depicting number of islands (log scale) and their respective island length for all significant islands (bp in log scale) identified in the WT (blue) and *Fmr1* KO (green) ChIP-seq. The island lengths were parsed in bins of 100bp and the center of each bin is plotted in the histogram. Asterisks indicate statistical significance.

(F) Scatter plot comparing the $\log_2$FC in RNA-seq (x-axis) with the ChIP-seq data (y-axis) averaging H3K36me3 island differences within each gene is plotted. Pearson correlation coefficient value is stated.

A

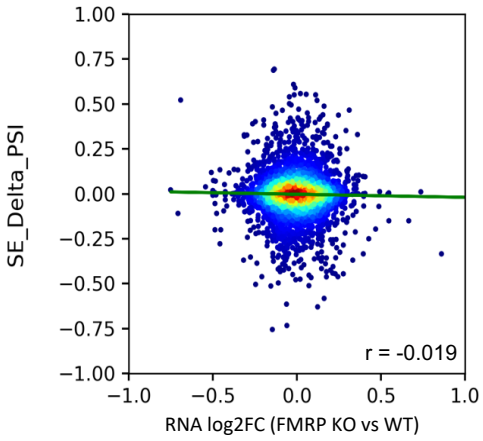
SE_Delta_PSI
RNA log2FC (FMRP KO vs WT)
r = -0.019

B

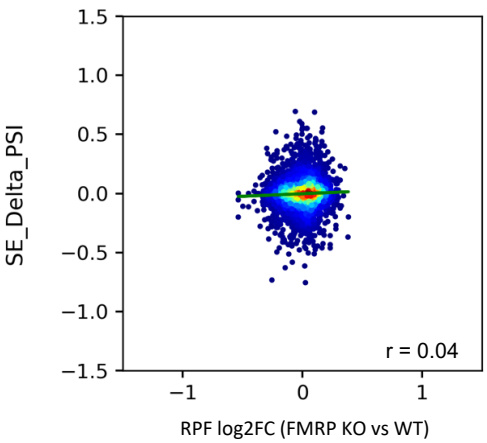
SE_Delta_PSI
RPF log2FC (FMRP KO vs WT)
r = 0.04

C

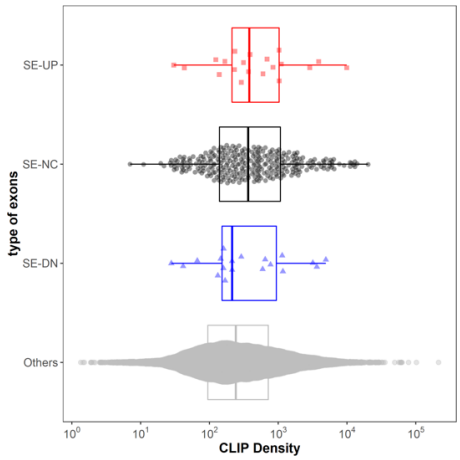
SE-UP
SE-NC
SE-DN
Others
type of exons
CLIP Density

D

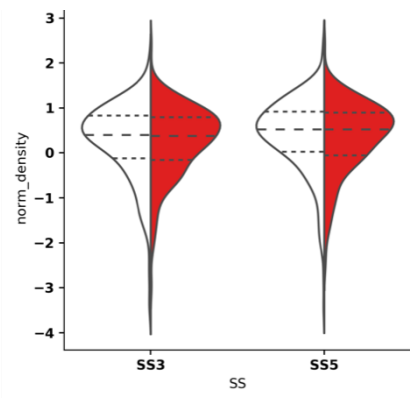
norm_density
SS3
SS5
SS

+/-150nt

E

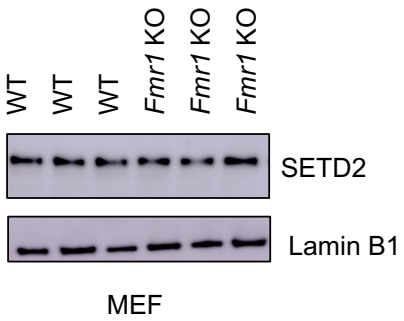
WT
WT
WT
Fmr1 KO
Fmr1 KO
Fmr1 KO
SETD2
Lamin B1
MEF

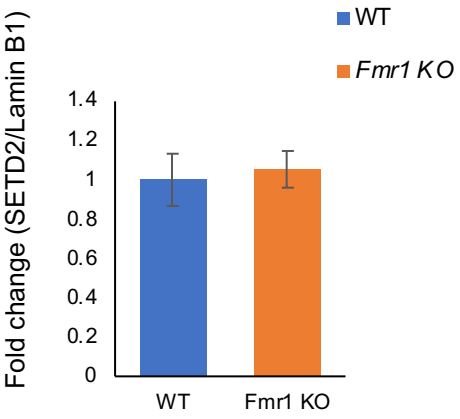
WT
Fmr1 KO
Fold change (SETD2/Lamin B1)
WT
Fmr1 KO

**Figure S5. Comparison of skipped exon genes to RNA abundance and RPF levels (Related to Figure 1,6, and 7 also see Table S1 and S3)**

(A) Scatter plot for the delta percent spliced-in (Psi/Ψ) score of skipped exons (y-axis) (From Figure 7) versus their RNA fold changes (From Figure 1) on the x axis. Pearson correlation coefficient value is stated.

(B) Scatter plot for the delta percent spliced-in (Psi/Ψ) score of skipped exons (y-axis) (From Figure 7) versus their RPF levels (From Figure 1) on the x axis. Pearson correlation coefficient value is stated.

(C) Swarm plots are shown representing the FMRP CLIP density (CLIP level/length) using the FMRP CLIP-Seq data (GSE45148) at skipped exons and their flanking introns of genes with increased exon skipping (SE-UP in red), decrease skipped exons SE-DN in blue) and no significant change in skipped exons (SE-NC) are plotted. The other category represents exons with no alternative splicing detected. Wilcoxon test was used to determine significance of differences amongst the categories.

(D) Violin plot for the H3K36me3 ChIP signal +/-150nt at the 5' (SS5) and 3' (SS3) splice sites of the alternatively skipped exons in WT (white) and *Fmr1* KO (red) hippocampus tissue (p-value<0.05, Wilcox test for significance). Also see Figure 7F.

(E) Western blot analysis of SETD2 and Lamin B1 in immortalized MEFs from WT and *Fmr1* KO mice (left), passage number 31. When quantified and made relative to Lamin B1 (right), there was no observable change in SETD2 levels in the *Fmr1* KO (3 replicates, p=0.48, two-tailed t test). Error bars represent the S.E.M (also see Figure 5)